IMPACT PERFORATION OF THIN CFRP LAMINATES

M. S. Found, I. C. Howard and A. P. Paran*

Static indentation and impact tests have been conducted on thin CFRP panels of different thicknesses and diameters. The impact perforation threshold energy may be estimated from the work done by the indentor during a static indentation test. Damage maps suggest that changes in failure mechanisms progressively occur up to the perforation threshold energy. The influence of membrane bending has also been identified.

INTRODUCTION

If composite materials are to remain competitive with advances in metallic alloys for aerospace applications it is important that designs are enhanced and manufacturing costs reduced. Frequently full-scale components and structures are fabricated and tested as part of the design evaluation process. This is expensive and time consuming and alternative routes are required if composite materials are to maintain or improve their market share. One way forward is to try to predict the behaviour of large components and structures from small-scale laboratory tests.

Attempts to model perforation of CFRP have been undertaken by a number of workers (1-3) using energy considerations. Cantwell and Morton (2) showed that elastic deformations, delaminations and shear-out were the main mechanisms, whilst Delfosse and Poursartip (3) suggested that matrix damage (30%) and fibre damage (70%) is absorbed at perforation. This paper suggests a means of predicting the impact perforation threshold energy, and hence to identify the principal failure mechanisms, based on the static perforation energy associated with a static indentation test.

*SIRIUS, Department of Mechanical Engineering, University of Sheffield.

EXPERIMENTAL

The material was a five-harness satin weave carbon fibre preimpregnated with an epoxy resin designated 914C-713-40 and supplied by Hexcel Composites. The panels were laid up as three-ply, six-ply and nine-ply laminates based on a three-ply sub-laminate (0/90, ±45, 0/90) together with four-ply (0/90, $\pm 45_2$, 0/90) and five-ply (0/90, ±45, 0/90, ±45, 0/90) laminates. The laminates were autoclave moulded by Hurel-Dubois UK at a nominal 58% fibre volume fraction. An instrumented dropweight impact rig, described in Refs. (4, 5), was used for both static indentation tests and low velocity impact tests. The panels were clamped to the same ring pressure using two annular rings ranging from 100 to 300 mm internal diameter. Dropweight impact tests were conducted from a height of 0.5 m to produce an impact velocity of the impactor of about 3 m/s. The impact forces and displacements were obtained from data that was processed through a low-pass filter at a cut-off frequency of 3.5 kHz (5). Damage was assessed using x-radiography and microscopy techniques in order to determine the principal failure mechanisms of delaminations, backface cracking and permanent indentation of the frontface.

RESULTS AND DISCUSSION

Figure 1 shows a typical force-displacement plot for a three-ply laminate of 300 mm diameter obtained from a static indentation test. In an attempt to identify possible relationships in terms of perforation of the panel the data has been normalised to the peak static force. Also shown is the normalised work done by the indentor during the test. Often the peak force is not as clearly defined as indicated here and therefore an average peak force is determined. This is obtained from the area under the force-displacement curve from initial damage load to the corresponding position on the downside of the plot. The initial damage load is identified by the first change in the upside of the plot which occurs at approximately 72% of the peak force shown in Figure 1. The static perforation energy of the panels may be estimated in terms of maximum work done by the indentor to produce upperbound and lowerbound values. The former is obtained from the crossover of the two plots in Figure 1 which occurs at approximately 82% of the maximum work done to give an estimated static perforation energy of 2.50 J. The lower value is determined from the work done by the indentor at the median displacement associated with the average peak force which occurs at approximately 60% of the maximum work done to produce an estimated static perforation energy of 1.82 J. The initial damage is in the form of backface cracking and remains dominant up to about the average peak force when delaminations become dominant. At the start of the downside of the load-displacement plot fibre fracture is significant leading to perforation of the panel.

In order to identify the effect of panel thickness and diameter on the force-displacement behaviour we used an approximate analysis (6) for thin isotropic panels which account for membrane bending and is given by

$$\frac{w}{h}+A\left(\frac{w}{h}\right)^3 = B.\frac{Pa^2}{Eh^4} \qquad (1)$$

where P is the force, E is Young's modulus, a is the panel radius, h is the thickness, w is the central displacement and A and B are constants. Encouragingly the data for all the tests almost collapse onto a single curve as shown in Figure 2. Furthermore, the data are bounded by two of the four end conditions considered by Timoshenko (6), namely an upperbound when the panels are clamped with moveable edge (CME) and a lowerbound of simply supported with moveable edge (SME). Clearly this first estimate will permit the prediction of the force-displacement response of large structural panels.

The static perforation energy also appears to be related to the impact perforation threshold energy as shown in Figure 3. There is some scatter in the data mainly arising from the variation in the static perforation energy which appears to have a range of values as discussed above. In this plot the upperbound value has been used to estimate the static perforation energy. Figure 3 also identifies the influence of panel diameter, with importantly the larger 300 mm panels having greater impact perforation energies than the smaller 100 mm panels. This highlights the very limited use of such small samples for trying to predict the response of large structural panels. It also shows that large structural panels should be capable of achieving greater damage tolerance than is often realised. Static and impact perforation energies are compared in Table 1 for three and nine-ply laminates of 100 and 300 mm diameter. The results show that as the panel size increases the lowerbound static perforation energy tends towards the upperbound value.

TABLE 1 Comparison of Lower and Upperbound Static Perforation Energies With Impact Perforation Energies

Laminate	Three-ply		Nine-ply	
Panel diameter mm	100	300	100	300
Static perforation Energy J	1.22	1.82	5.80	10.48
	2.02	2.50	11.41	13.11
Impact perforation Energy J	2.40	2.90	10.90	13.40

We have previously presented (4) energy maps as a means of identifying the different mechanisms that develop from initial damage to perforation for panels subjected to impact. In this paper we have taken these damage maps a stage further by normalising both the damage parameters and the incident kinetic energy to their respective values associated with the onset of perforation of the panels as shown in Figure 4 for panels of 100 mm diameter. There are four distinct regions where different mechanisms appear to dominate the impact behaviour. In the first region, from onset of damage up to 50% of the perforation threshold energy, backface cracking is dominant. In the second region, 50 to 75% of the perforation threshold energy, the growth of delaminations is the dominant mechanisms. The third region is controlled by increase in fibre fractures and occurs from 75% to the onset of perforation of the panel. Finally,

region four is of increasing levels of perforation which do not appear to cause further increase in size of the main damage parameters. In this programme of work the change in failure mechanisms, as identified by the four regions, occur at approximately similar proportions of the perforation energy for panels of different diameters and thicknesses. Figure 4 also shows that the thinner three-ply panels exhibit proportionally much less total backface cracking than the nine-ply panels and slightly lower delaminations, although of course for the same actual kinetic energy the size of the damage is greater in the thinner panel. This apparent change in damage parameter is thought to be caused by the additional membrane bending associated with the thinner panels. It will also be noted that the onset of damage occurs at a greater normalised kinetic energy for the three-ply panels.

In Figure 5 an energy map is presented for frontface panel damage in the form of permanent indentation. Similar trends in the data for the panels of different thicknesses can be related to the changes in mechanisms associated with Figure 4. For example, in the first region from onset of damage to 50% of the perforation threshold energy all of the data appears to have a common linear relationship. In the second region the relationship remains linear but of increasing rate for each panel thickness. It is only in the third region beyond 75% of the onset of perforation that the data diversifies with the thinner panel having a proportional greater increase in indentation.

CONCLUSIONS

The results presented suggest means of being able to predict the impact response of large thin CFRP panels based on information from static indentation tests of laboratory scale. The static perforation energy may be estimated from the work done by the indentor and the values used to estimate the impact perforation threshold energy. Changes in failure mechanisms have been identified where backface cracking, delamination and fibre fracture are dominant at successive stages leading to impact perforation. The influence of membrane bending has been identified in both static and impact tests.

REFERENCES

(1) Dovey, G., Proc. 6th Int. Conf. on Composite Matls., Elsevier Appl. Sci., 1987, pp. 3.1-3.26.

(2) Cantwell, W. J. and Morton, J., Composites Sci. & Technol., 38, 2, 1990, pp. 119-141.

(3) Delfosse, D. and Poursartip, A., Composites, 28A, 1997, pp. 647-655.

(4) Found, M. S., Howard, I. C. and Paran, A. P., Composite Struct., 38, 1997, pp. 599-607.

(5) Found, M. S., Howard, I. C. and Paran, A. P., Composite Struct., 1998, in press.

(6) Timoshenko, S. P. and Woinowsky-Krieger, S., Theory of Plates and Shells, 2nd Edn, McGraw-Hill, 1970, pp. 396-415.

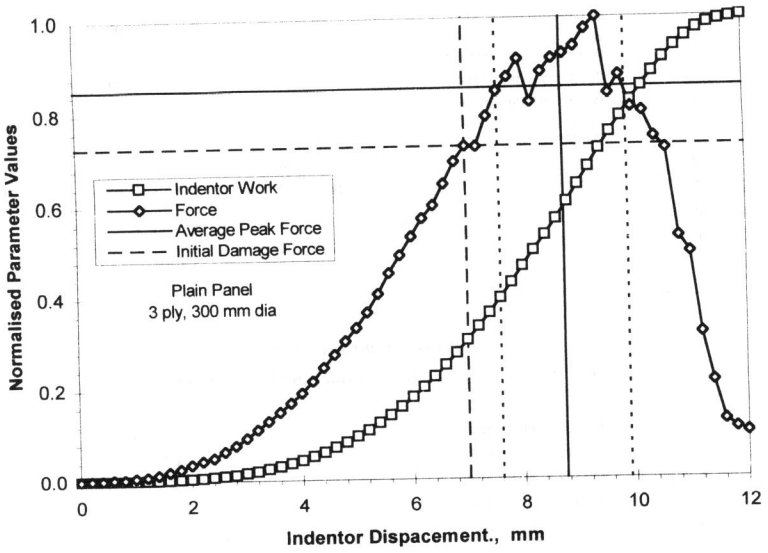

Figure 1 Normalised static indentation plots.

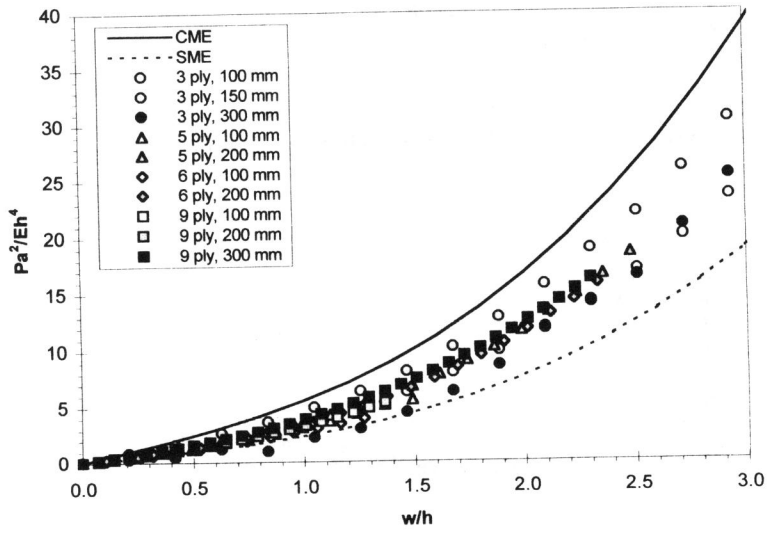

Figure 2 Non-dimensional force-displacement analysis using Eqn. (1).

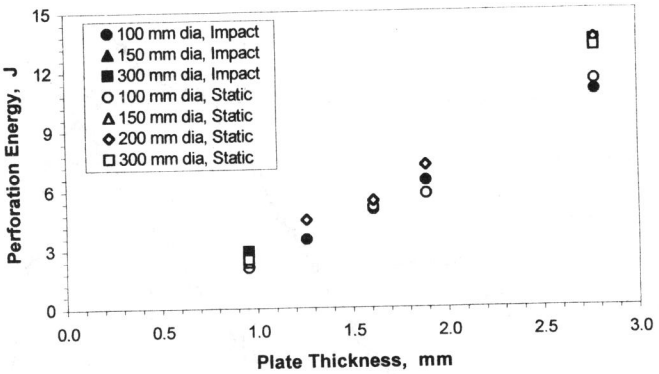

Figure 3 Static and impact perforation energies.

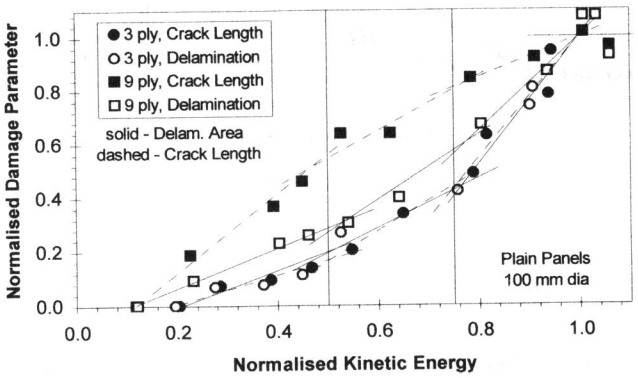

Figure 4 Backface crack length and delamination area.

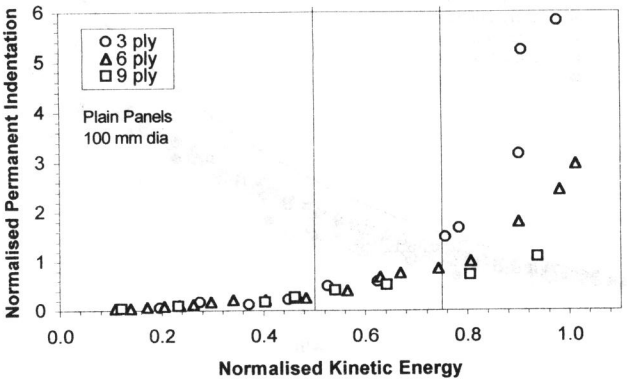

Figure 5 Permanent indentation of frontface.